RSC Advances

PAPER

Cite this: *RSC Adv.*, 2020, **10**, 40206

Hyperthermia evaluation and drug/protein-controlled release using alternating magnetic field stimuli-responsive Mn–Zn ferrite composite particles

Wararat Montha,[a] Weerakanya Maneeprakorn,[b] I-Ming Tang[c] and Weeraphat Pon-On*[a]

Drug delivery particles in which the release of biomolecules is triggered by a magnetic simulant have attracted much attention and may have great potential in the fields of cancer therapy and tissue regenerative medicine. In this study, we have prepared magnetic Mn–Zn ferrite ($(Mn,Zn)Fe_2O_4$) (MZF) nanoparticles coated with chitosan-*g*-*N*-isopropylacrylamide (Chi-*g*-NIPAAm) polymer (MZF@Chi-*g*-NIPAAm) to deliver the anticancer drug (Doxorubicin, DOX) and bioactive proteins (Bone morphogenic protein (BMP-2)-immobilized bovine serum albumin (BSA)) (P//MZF@Chi-*g*-NIPAAm) and be used as chemo-hyperthermia and vector delivering biomolecules. For these purposes, we first show that the as-prepared MZF@Chi-*g*-NIPAAm particles exhibit super paramagnetic behavior and under certain conditions, they can act as a heat source with a specific absorption rate (SAR) of 34.88 W g^{-1}. Under acidic conditions and in the presence of AMF, the fast release of DOX was seen at around 58.9% within 20 min. *In vitro* evaluations indicated that concurrent thermo-chemotherapy treatment by DOX-MZF@Chi-*g*-NIPAAm using AMF had a better antitumor effect, compared with those using either DOX or DOX-MZF@Chi-*g*-NIPAAm without AMF (89.02% of cells were killed as compared to 71.82% without AMF exposure). Up to 28.18% of the BSA (used as the model protein to determine the controlled release) is released from the P//MZF@Chi-*g*-NIPAAm particles under AMF exposure for 1 h (only 17.31% was released without AMF). These results indicated that MZF@Chi-*g*-NIPAAm particles could be used to achieve hyperthermia at a precise location, effectively enhancing the chemotherapy treatments, and have a promising future as drug or bioactive delivering molecules for cancer treatment and cartilage or bone regenerative applications.

Received 9th October 2020
Accepted 23rd October 2020

DOI: 10.1039/d0ra08602a

rsc.li/rsc-advances

1. Introduction

Nanoparticle delivery systems consisting of biocompatible super paramagnetic materials and bioactive molecules having a variety of thermo-chemotherapy potentials are used as therapeutic cancer treatment agents and to regenerate cartilage or bone tissue.[1–7] Based on their separate roles, a combination of magnetic actuation, local heating and controlled release would help to achieve better efficacy for active targeting for treatment and be less toxic to healthy tissue. Over the past decade, magnetic ferrite (MFe_2O_4, M = Fe, Mn, Co) combined with stimuli-responsive polymers, which can change their structure and physicochemical properties when exposed to external and internal stimuli, have successfully been developed to provide selective drug/biomolecule delivery capabilities.[8–12] To improve the efficacy, the controlled release of the drugs/biomolecules where they would be needed can be triggered by light, heat, enzyme, pH, electromagnetic field *etc.*[10–12] applied at the desired location. Among the numerous triggered controlled release methods, an alternating magnetic fields (AMF) is often used since it would provide for stimuli-controlled release at high depths inside the human body. The lack of radiotoxicity of the AMF radiation makes for the safety of this procedure.[8,13,14] Upon application of the AMF to the biocompatible magnetic particles, a small increase in the intensity of the radiation would promote the release of the drug from the delivery vehicle, while the rise in the temperature (magnetic hyperthermia) of the surrounding media to clinical hyperthermia levels (41–46 °C) could be used for possible cancer therapy applications.[13,15,16] Magnetic hyperthermia has been studied as a means for triggering the differentiation of cancer cells. For example, Moise S. *et al.*,[17] reported that magnetic hyperthermia not only triggering heat related cell

[a]*Department of Physics, Faculty of Science, Kasetsart University, Bangkok 10900, Thailand. E-mail: fsciwpp@ku.ac.th*

[b]*National Nanotechnology Center (NANOTEC), National Science and Technology Development Agency (NSTDA), Pathum Thani 12120, Thailand*

[c]*Computational & Applied Science doe Smart Innovation Clusters, Faculty of Science, King Mongkut's University of Technology, Thonburi, Bangkok 10140, Thailand*

death but also provided an additional stimulus to the surviving cells to further differentiate to form a more mature phenotype. Not only magnetic particles were used in cancer drug delivery and hyperthermia treatment but also, they have also been used for vectoring biomolecules such as proteins or growth factors (GFs) to target the defect sites of such cartilage and bone.[18–22] There have been reports on the use of magnetic particles for growth factor delivery. Ming. F. *et al.*[19] showed that the magnetic Fe_3O_4-biopolymer nanogel vectoring delivery of BMP-2 could be controlled by the external magnetic field and that these particles have high efficiency for promoting MG-63 cells viability. This last property points to a promising future for its use in cartilage and bone regeneration applications. Gwangjun G. *et al.*,[6] showed the capability of mesenchymal stem cell (MSC) delivery for cartilage by using super paramagnetic microporous combined with an electromagnetic actuation. The results of this study demonstrated that magnetically actuated microporous scaffolds carrying MSC driven by external magnetic field have a potential for cartilage regeneration. In this work, we study the response of $(Mn,Zn)Fe_2O_4$ to the AMF, which will act as anticancer drug delivery and vectoring delivery of BMP-2-immobilized BSA. We have coated these particles with thermo responsive chitosan (chitosan-*g*-*N*-isopropylacrylamide (Chi-*g*-NIPAAm) polymer) which will be the matrix for chemical drug (DOX) and protein (BMP-2-immobilized BSA) being loaded on them. The Mn–Zn ferrites were chosen since they have a higher specific absorption rate (SAR) to the AMF than the others ferrites.[23–27] It should to noted that Fe, Mn and Zn are all biocompatible elements (in fact they are essential trace nutrients). Yang Q. *et al.*,[23] found that the (Mn,Zn) nano ferrite with the composition of $Mn_{0.6}Zn_{0.4}Fe_2O_4$ could be employed in magnetic hyperthermia treatment and their use resulted in cancer cell death rate up to 90% within 15 min. Xie J. *et al.*,[24,25] found that their multi-modal Mn–Zn ferrite nanoparticles achieved promising tumor therapeutic results. Jović Orsini N. *et al.*,[26] studied Zn and Mn substituted magnetite nanoparticles and showed that the best heating performance with the specific absorption rate (SAR) ≈ 425 W. Meanwhile, chitosan and *N*-isoproyplacrylamide (and their co-polymer Chi-*g*-NIPAAm) are commonly used pH-responsive and thermo-responsive polymers and there are biodegradable, allows high capacity of biomolecules loading, controlled release and safety in clinics.[28–30] Meanwhile, the growth factors, especially bone morphogenic proteins (BMPs) have been widely used because they play important roles in bone and cartilage regeneration.[31–33] Thus, the localized and sustained delivery of BMP-2 to the defect site would further enhance the regenerative capacity which may be applied to cartilage or bone tissue regeneration applications. To examine whether this MZF@Chi-*g*-NIPAAm particles could be an effective drug/protein delivery system in which the AMF would control the release of the DOX drug in the chemo-hyperthermia therapy treatment of cancer, we studied its physical properties and *in vitro* therapeutic efficiency. For vectoring delivery and controlled protein release, the release of BMP-2-immobilized BSA protein under influence of AMF was investigated. The DOX-MZF@Chi-*g*-NIPAAm nano particles, which had been exposed to an AMF (3 A, 100 kHz) for 30 min, had the best (most efficient) anti-cancer ability, *e.g.*, they produced a cell viability of 10.98% compared to 28.18% without AMF exposure. The preliminary results indicate that DOX-loaded MZF@Chi-*g*-NIPAAm could achieve the best synchronization of the hyperthermia and chemotherapy mechanism, leading to better enhancement of the combined antitumor efficacy. This is due to the fact the application of an alternating magnetic field to P@MZF@Chi-*g*-NIPAAm particles result in an enhanced BSA release from particles. Based on these results, we concluded that this approach would be the most promising procedure for achieving both the targeted delivery and controlled release of biomolecules.

2. Materials and methods

2.1. Materials

Ferric chloride ($FeCl_3$ anhydrous), manganese nitrate ($Mn(NO_3)$ $4H_2O$) and zinc nitrate ($(Zn\ (NO_3))_2 \cdot 6H_2O$) were obtained from UNIVAR (Australia). The sodium dodecyl sulfate (SDS), Na_2SO_4, chitosan, *N*-isopropylacrylamide, citric acid, and ethylene glycol (EG) were obtained from Fluka (Switzerland). All chemicals used were of analytical grade and were used without further purification. The water used throughout this work was deionized water. In the experiments on drug loading and drug release, doxorubicin (DOX) (Fluka, Biochemika) was used as a model anticancer drug. For bioactive protein release study, bone morphogenic protein (BMP-2) (Fluka, Biochemika) and bovine serum albumin (BSA) (Fluka, Biochemika) were used to model the proteins. Phosphate buffered saline (PBS) (Fluka, Biochemika) was used in the protein and drug solution. To study the response of $(Mn,Zn)Fe_2O_4$ to the AMF, we coated these particles with thermo responsive chitosan (chitosan-*g*-*N*-isopropylacrylamide (Chi-*g*-NIPAAm) polymer) so that the chemical drug doxorubicin (DOX) and bioactive proteins (Bone morphogenic protein (BMP-2)-immobilized bovine serum albumin (BSA)) could be loaded onto them (Scheme 1).

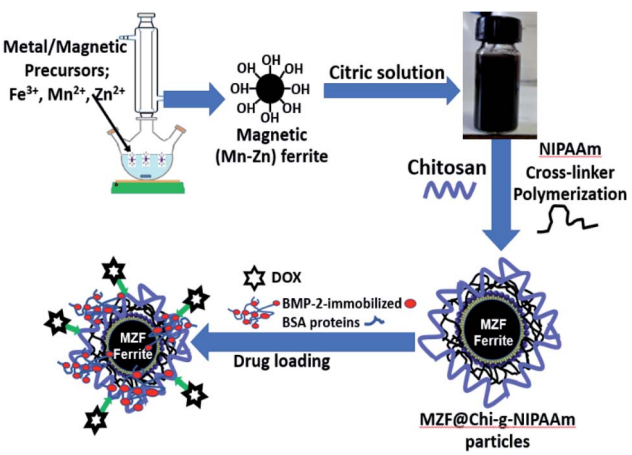

Scheme 1 Illustration of the synthesis of $(Mn,Zn)Fe_2O_4$ particles coated with thermo responsive chitosan (chitosan-*g*-*N*-isopropylacrylamide (Chi-*g*-NIPAAm) polymer) and chemical drug doxorubicin (DOX) and bioactive proteins (Bone morphogenic protein (BMP-2)-immobilized bovine serum albumin (BSA)) loading.

2.2. Preparation of (Mn,Zn) Fe_3O_4 (MZF) nanoparticles

Magnetic (Mn,Zn)Fe_2O_4 particles were synthesized by prepared using the alkaline co-precipitation method based on previous reports and steps used are given in our reports.[23,34] In brief, nitrate salt of $Mn(NO_3)4H_2O$ (0.9 mmol), $Zn(NO_3)_26H_2O$ (0.1 mmol) and $FeCl_3$ anhydrous (2 mmol) were dissolved in and mixed in 50 mL deionized water, ethylene glycol (EG, 10 mL) and 5 mL of 0.2 M HCl under vigorous stirring. The solution was stirred for an addition 30 min at room temperature. Then, the mixing salt solution was added dropwise into a 250 mL round bottom flask containing 3 g of NaOH and 0.54 g of SDS which were dissolved in 25 mL of distilled water at 80 °C under magnetic stirring for 30 min. At the end of reaction, (Mn,Zn) Fe_2O_4 particles were collected by an external magnetic field and washed three times with ethanol and deionized water. To obtain the activation of carboxyl groups of (Mn,Zn)Fe_2O_4 particles, pre-dissolved citric acid solution (0.05 M) was added to the magnetic particles producing the carboxylic functional (Mn,Zn) Fe_2O_4 (MZF). The nano particles were obtained by freeze drying.

2.3. Preparation of thermo-responsive chitosan (chitosan-*g*-*N*-isopropylacrylamide (Chi-*g*-NIPAAm)) coated (Mn,Zn) Fe_2O_4 nanoparticles and doxorubicin (DOX) drug loading

For coating the MZF particles with the Chi-*g*-NIPAAm polymer, 0.5 g of citric acid-modified (Mn,Zn)Fe_2O_4 particles were dispersed in 15 mL of chitosan in acetic acid (1 wt% of chitosan in 2.5 wt% of acetic acid). Then, the chitosan-magnetic solution was added drop wise into 50 mL of solution of NIPAAm (0.5 g) and MBA (0.01 g) mixed under N_2 atmosphere/70 °C. After 30 min, the ammonium persulfate (APS) solution (0.02 g/10 mL deionized water) was added slowly into the solution and held for 6 h. Finally, the obtained particles were collected by magnetic field and washed several times with deionized water and the final MZF@Chi-*g*-NIPAAm particles were obtained by freeze drying. For loading doxorubicin (DOX), 50 mg of MZF@Chi-*g*-NIPAAm particles were dispersed in 5 mL PBS at pH of 7.4 and then 1 mL of DOX solution (1 mg mL^{-1}) was added and stirred continuously at room temperature overnight under dark condition. After centrifuging, the supernatant was discarded and the precipitate was washed with deionized water repeatedly three times. The resulting DOX-loaded MZF@Chi-*g*-NIPAAm products were freeze-dried and stored in a refrigerator at 4 °C for further investigations.

2.4. Preparation of bioactive proteins BMP-2-immobilized BSA loading MZF@Chi-*g*-NIPAAm particles (P//MZF@Chi-*g*-NIPAAm)

To loaded BMP-2-immobilized BSA proteins into the MZF@Chi-*g*-NIPAAm particles (P//MZF@Chi-*g*-NIPAAm), 0.25 mg mL^{-1} MZF@Chi-*g*-NIPAAm particles was immersed in protein solution consist of BMP-2 with 10 μg mL^{-1} and 100 μg mL^{-1} of BSA in PBS solution under magnetically for 4 hours. At the end of reaction, the P//MZF@Chi-*g*-NIPAAm particles were collected with magnet, the supernatant removed and the obtained powders were washed several times for removal residual proteins. Subsequently, the obtained BMP-2-immobilized BSA proteins with the MZF@Chi-*g*-NIPAAm powder by freeze dried and then stored at 4 °C before they were subjected to the next application and analysis.

2.5. Physicochemical characterization of the MZF@Chi-*g*-NIPAAm particles

The crystallographic structures of the synthesized MZF and MZF@Chi-*g*-NIPAAm powders were determined by powder X-ray diffraction (XRD) (Bruker diffractometer, Model D8 Advance) using the Cu Kα radiation. The XRD patterns were scanned between $2\theta = 20°$ and 70° with an increment of 0.037° per step. The magnetic properties of (Mn,Zn)Fe_2O_4 and MZF@Chi-*g*-NIPAAm particles were measured using a room temperature VSM (vibrating sample magnetometer (Lakeshore, Model 4500)). The as-prepared MZF powder and composite nanoparticles were examined by a transmission electron microscope (TEM) (TEM-Hitachi HI7700), one drop dispersed solution of MZF and MZF@Chi-*g*-NIPAAm were deposited on carbon grids.

2.6. Magnetic heating and *in vitro* AMF stimulating drug/protein release studies

The magnetic heating efficiency of MZF@Chi-*g*-NIPAAm particles was evaluated by using a homemade AC current generator operating at 100 kHz with the current of 3 A. Magnetic heating measurement, 3 mL of the dispersed solution of MZF@Chi-*g*-NIPAAm particles in water with the concentration of 1 mg mL^{-1} was placed inside the middle of 6-turn copper coil with 30 mm in diameter and 65 mm in length and current is passed through a coil. The heat generated by the sample was investigated by measuring the change in temperature of solution (using the alcohol thermometer placed at the central of suspension) as function of time up to 60 min.

To determine the drug release under exposed to magnetic field stimulating, the *in vitro* study of controlled DOX and BMP-2-immobilized BSA release from the MZF@Chi-*g*-NIPAAm nanoparticles was performed as follows: first, 1 mg of DOX-MZF@Chi-*g*-NIPAAm or P//MZF@Chi-*g*-NIPAAm particles was placed in 3 mL of phosphate buffer solution (PBS) (pH = 5.5 for DOX release and pH = 7.4 for BMP-2-immobilized BSA release). After passage of a time intervals (1, 5, 10, 20, 30 and 60 min), 1 mL of the released medium was extracted from the solution and replaced with an equal volume of fresh buffer solution. The amounts of DOX and BSA (a model protein release) released into the original buffer solution were determined using UV-visible spectrometer (Jenway, model 6405) at a wavelength of 480 nm and 240 nm, respectively.

2.7. Cell culture and *in vitro* cytotoxicity (chemo-hyperthermia) of DOX-loaded MZF@Chi-*g*-NIPAAm particles

To evaluate the effect of chemo-hyperthermia test, human cervical cancer cells (HeLa cells) was used and the culture was found in our previous work.[34] The cultured cells were kept at 37 °C in a humidified CO_2 incubator during cultivation and during the experiments. For the cytotoxicity analysis of the particles with or without AMF treatment, HeLa cells were

seeded in 96-well plates and then incubated with DOX, MZF@Chi-*g*-NIPAAm and DOX-MZF@Chi-*g*-NIPAAm suspensions in media at a concentration of 250 μg mL^{-1}. For the AMF-triggered chemo-hyperthermia therapy, the cells that were incubated with particles were exposed to a homemade AC current generator operating at 100 kHz with the current of 3 A for 10 min. At certain time intervals, cell viability was assessed by MTT assay in which 100 μL 3-[4,5-dimethylthiazol-2-yl]-2,5-diphenyl-tetrazolium bromide (MTT) solution was added to each well and incubated for another 2 h. Then the absorbance intensity of each well was measured with a micro plate reader (Varioskan LUX, Thermo Fisher Scientific Inc. Waltham, Massachusetts, USA) at the excitation and emission fluorescence at 560 and 590 nm, respectively. The cytotoxicity was expressed as the percentage of cell.

3. Results and discussion

Transmission electron microscopy (TEM) was used to investigate the nanostructure of as-prepared $(Mn,Zn)Fe_2O_4$ (MZF) nanoparticles and the samples which consist of a magnetic core and polymer shell. As seen in Fig. 1(a), the as-synthesized magnetic nanoparticles exhibit a monodispersed spherical morphology of uniform size of about 15 nm. After mixing the magnetic particles with Chi-*g*-NIPAAm, the composite structure of MZF@Chi-*g*-NIPAAm can clearly be seen Fig. 1(b). The dark particles surrounded by thin polymer shells are clearly seen in each particle.

The number-averaged size of as-prepared particles was determined by dynamic light scattering (DLS). The results showed the average particle diameter of 42 nm for Mn–Zn ferrite ($(Mn,Zn)Fe_2O_4$) (MZF) nanoparticles (Fig. 1(c)) and was found to be 0.65 μm for MZF@Chi-*g*-NIPAAm particles (Fig. 1(d)), which was larger than that observed by TEM (Fig. 1(a) and (b)). The increasing average particle diameter after polymer coating is due to the agglomeration of MZF@Chi-*g*-NIPAAm particles owning to the magnetic nature of composite particles. The XRD patterns show that the $(Mn,Zn)Fe_2O_4$ nanoferrites have a single-phase cubic spinel ferrite structure and do not exhibit any undesirable crystalline phase. The diffraction peaks at about 30.2, 35.6, 43.0, 57.1 and 62.5° which are due to reflection from the (220), (311), (400), (511) and (440) planes, respectively, are clearly observed. These peaks correspond to the peaks of ferrites (JCPDS file of PDF 00-022-1012).[23] After coating the ferrites with Chi-*g*-NIPAAm, the XRD intensities decreased slightly, this being due to the attenuation of the X-ray by the polymer coating the $(Mn,Zn)Fe_2O_4$ particles (Fig. 2).

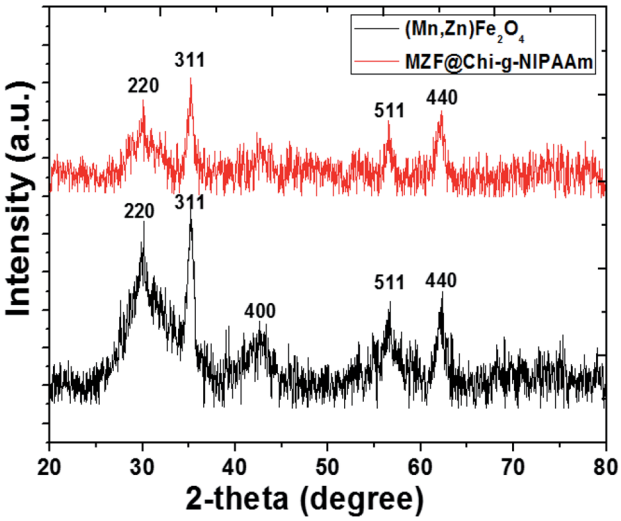

Fig. 2 XRD patterns of as-prepared $(Mn,Zn)Fe_2O_4$ (MZF) nanoparticles and MZF@Chi-*g*-NIPAAm particle.

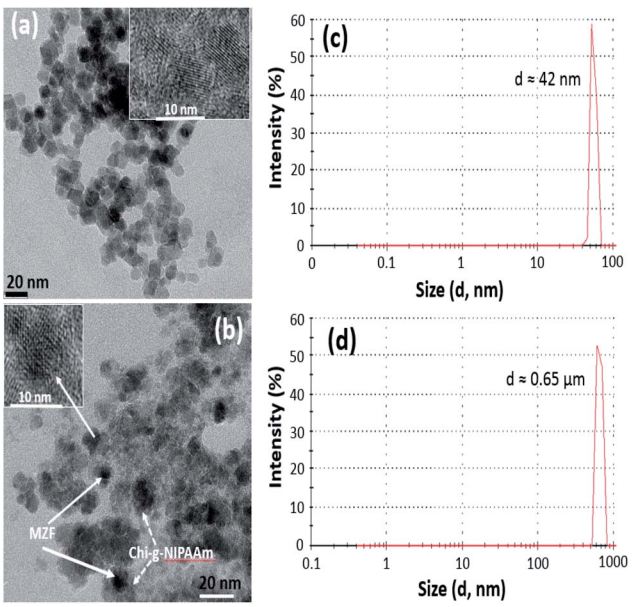

Fig. 1 TEM image of the as-prepared $(Mn,Zn)Fe_2O_4$ (MZF) nanoparticles (a) and MZF@Chi-*g*-NIPAAm particle (b). DLS average particle diameter of MZF nanoparticles (c) and MZF@Chi-*g*-NIPAAm particles (d).

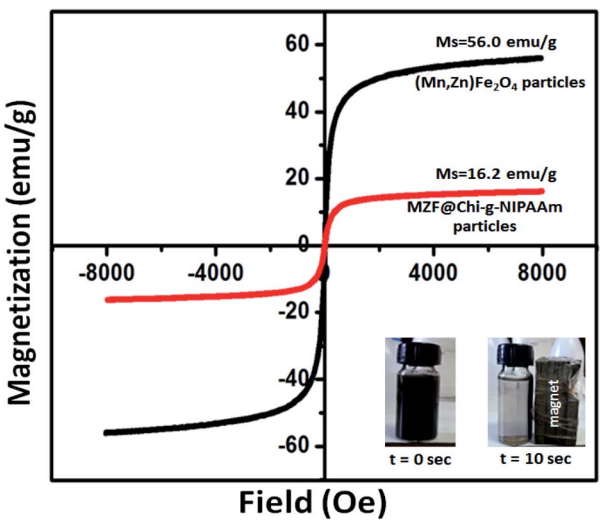

Fig. 3 Magnetization curves of the as-synthesized $(Mn,Zn)Fe_2O_4$ (MZF) nanoparticles and MZF@Chi-*g*-NIPAAm particles at room temperature.

The room-temperature magnetization curves of (Mn,Zn)Fe_2O_4 and MZF@Chi-*g*-NIPAAm are shown in Fig. 3. The magnetic hysteresis curves of the different synthesized particles do not exhibit any coercivity (H_c) or remanent magnetization (M_r) which are expected of paramagnetic materials. They do however exhibit a saturation magnetization (M_S) showing that all of them have super paramagnetic properties at room temperature. The M_S of (Mn,Zn)Fe_2O_4 (56.0 emu g^{-1}) nanoparticle is higher than that of MZF@Chi-*g*-NIPAAm (16.2 emu g^{-1}) nanoparticles. The cause of this is the presence of the polymer shell in the latter nanoparticles. These components contribute to the mass but not to the magnetization. Even though the magnetizations of the MZF@Chi-*g*-NIPAAm would be less than that of the uncoated substrate, the MZF@Chi-*g*-NIPAAm particles still have good magnetic responsiveness (inset in Fig. 3). This means that these coated nanoparticles can still be affected by an external magnetic field gradient, opening up the possibility of them being immobilized (targeted to) at sites by placing an external magnetic field gradient at the sites.

To explore the magnetic heat-generation characteristic of MZF@Chi-*g*-NIPAAm particles was studied by dispersing the particles in water and subjecting them to an AMF of 3 A where the frequency is 100 kHz for 60 min. Fig. 4 shows the temperature *versus* time curve obtained after applying the AMF field, it shows the temperature increasing from 31.5 to 36.0 °C ($\Delta T = 4.5$ °C) within 30 min. The concentration of the nanoparticles in the sample is about 1 mg mL^{-1}.

The hyperthermia performance is measured by the specific absorption rate (SAR) which is calculated from the heating efficiency of the nanoparticles from the formula given below:

$$\mathrm{SAR}\left(\mathrm{W\ g^{-1}}\right) = [C_w/m] \times [\mathrm{d}T/\mathrm{d}t] \quad (1)$$

where C_w is the specific heat capacity (4.186 J g^{-1} °C^{-1}) and m is the magnetic particle concentration. dT/dt is the slope of the temperature *versus* time curve. The initial slop of the temperature-dependent time curve was determined during the first 60 s and was 0.010 °C s^{-1}. Therefore, the SAR values for MZF@Chi-*g*-NIPAAm particle was calculated to be 34.88 W g^{-1}. It was found that the calculated SAR value of MZF@Chi-*g*-NIPAAm particles in this study is lower than those of previous iron-based nanoparticles developed for magnetic hyperthermia which have SAR values in range of 100–600 W g^{-1}.[23–27,35] The lower SAR in our result may be due to the relatively lower field strength (100 kHz AMF with the current of 3 A) which leads to decrease of contribution due to the macroscopic temperature (heat generation through Néel–Brownian relaxation due to fact synthesized particles exhibited no remanence). In general, the SAR value depends on the experimental conditions (frequency and magnetic field strength) and also on the intrinsic heating efficiency of magnetic nanoparticles which depends on the magnetization, anisotropy, size as well as the size distribution of the particles.[36,37] Thus, to achieve the optimal magnetic particles, parameters such as the frequency of the AFM signal and magnetic field strength must be tuned when the particles are used for magnetic hyperthermia treatment.

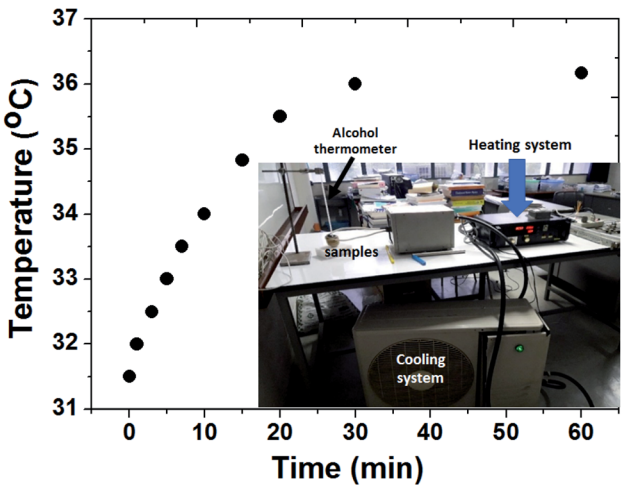

Fig. 4 Thermal responsive curves of MZF@Chi-*g*-NIPAAm particles dispersed in water with a concentration of 1 mg mL^{-1} and subjected to an AMF (f = 100 kHz and current of 3 A).

To study the controlled release and verify the effect of the AMF responsive release behavior of DOX drug from MZF@Chi-*g*-NIPAAm particles, the pH of the solution containing the as-prepared particle was set at 5.5. The AMF was turned on for 60 min (compared without exposure to an AMF). It is well known that chitosan is stable at the physiological pH level of 7.4, but is unstable in an acid environment. *N*-isopropylacrylamide (NIPAAm) is a thermos-responsive polymer which breaks down as the temperature is changed. As shown in Fig. 5, we have plotted the cumulative concentration of the drug DOX in the buffer solution as a function of time when the pH values are 5.5 and with or without AMF exposure. For the pH of 5.5 and without the AMF, the release of the DOX from MZF@Chi-*g*-NIPAAm particle is seen to be a sustained release with only 31.75% of DOX released after 60 min. When the AMF is on, the two types of behaviors observed are an initial small burst release during the first 20 min. This is followed by a sustained release after the 20 min. The initial burst release of DOX is attributed to the release of DOX molecules attached to the surface of particles. As seen for this case, the release of the nanocarriers is much faster and more complete then previously seen. The burst release from the MZF@Chi-*g*-NIPAAm particles during the first 20 min is about 58% which is around 1.8-fold higher than that of without AMF exposure. The amount of DOX released to the environment surrounding when the pH is 5.5 and the AMF external field is applied can be explained as being due to the agitation and disruption of coating polymer by the AMF. Under these conditions, the DOX molecules might diffuse through the channels formed when there is a disruption in the core/shell structure of the MZF@Chi-*g*-NIPAAm particles. The disruption of the particles might be due to the acidic pH-stimuli the protonation (amino group ($-NH_2$) yields $-NH_3^+$) of both the chitosan and NIPAAm polymers and the swelling, whereas it's deprotonation is in an alkaline environment. Meanwhile, the rising hyperthermia temperature due to magnetic field vibration stimuli can act as driving force to facilitate to diffusion of drug molecules from the channels. The inset in Fig. 5 shows the

TEM images appearing disruption of the MZF@Chi-*g*-NIPAAm particles during an external AMF to control the release of DOX.

In vitro cytotoxicity of the synthesized particles, the *in vitro* AMF stimuli-responsive property of DOX release leads us to use an external AMF to control the release of DOX to achieve better chemotherapy efficacy. To determine the cytotoxic effects of the DOX, MZF@Chi-*g*-NIPAAm and DOX-MZF@Chi-*g*-NIPAAm particles with or without AMF exposure against HeLa cells were measured. The results (Fig. 6) show that all the particles exhibited cell proliferation inhibition.

Without AMF exposure, the cytotoxic effects of all samples showed no significant cytotoxicity to cancer cells between the DOX and synthesized particles. Importantly, for the DOX-MZF@Chi-*g*-NIPAAm particles group, which were exposed to an AMF (3 A, 100 kHz) for 10 min, a more efficient anti-cancer effect was obtained with a cell viability of 10.98% compared to 28.18% without exposure (leads to 89.02% and 71.82% cell death, respectively). The cell viability of DOX and MZF@Chi-*g*-NIPAAm particles were 27.24% (30.12% without exposure to an AMF) and 21.13% (25.01% without exposure to an AMF), respectively. A significant decrease in cell viability when HeLa cells were treated with magnetic field after incubation with DOX-MZF@Chi-*g*-NIPAAm particles is attributed to the release of DOX triggered by the acidic environment in cells and DOX-MZF@Chi-*g*-NIPAAm particles had synergistic effect of chemo- and magnetic hyperthermia therapy. These finding probably facilitated the cellular uptake of DOX-MZF@Chi-*g*-NIPAAm particles *via* endocytosis and triggering release of DOX (targeted to the cell nucleus) into the cytosol led to DNA causing damage. Conclusively, these results suggestive that the DOX-MZF@Chi-*g*-NIPAAm particles with AMF could actively target cancer cells would therefore have great potential for targeting cancer tissues and enhancing chemotherapy *in vivo*.

As the vectoring delivery of protein, to determine the attachment of BMP-2-immobilized BSA to MZF@Chi-*g*-NIPAAm, FTIR spectra of MZF@Chi-*g*-NIPAAm and BMP-2-immobilized BSA loading MZF@Chi-*g*-NIPAAm as shown in Fig. 7. In the MZF@Chi-*g*-NIPAAm spectrum (Fig. 7(a)), peaks were identified at both 1652 cm^{-1}, 1410 cm^{-1}, 1080 cm^{-1} and 540–600 cm^{-1}, representing the electrostatic interaction due to $-NH^{3+}$ and $-COO^{-}$ between the chitosan and *N*-isopropylacrylamide (Chi-*g*-NIPAAm) polymer, methyl vibration, symmetric stretching of C–O–C and stretching vibrations of metals-oxide bonds (Fe–O, Mn–O or Zn–O), respectively.[30,34] For the P//MZF@Chi-*g*-NIPAAm (Fig. 7(b)), peaks were identified at 1664 and 1393 cm^{-1}, representing two different amide bonds.[40] These peaks indicate a successful conjugation because when BMP-2 is bound to the MZF@Chi-*g*-NIPAAm particle, a resonance effect is produced, moving the peaks to a lower frequency.[38,39]

The release profile of protein (BSA was used as protein model) from the MZF@Chi-*g*-NIPAAm particles were investigated in absence and presence in AMF stimulated at pH 7.4 as shown in Fig. 8(a). As control release test of our studied, the samples exposed to the magnetic field showed a 25.14% for BSA release in the first 30 min and 28.18% after 1 h of AMF exposure. Without the magnetic field, in the control sample, we observed that only 17.30% of the absorbed BSA on P//MZF@Chi-*g*-

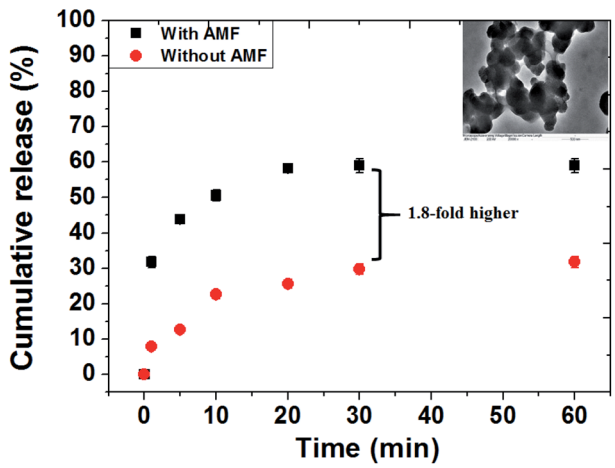

Fig. 5 *In vitro* drug release behavior from the DOX-MZF@Chi-*g*-NIPAAm particles at pH 5.5 in the presence of AMF ($f = 100$ kHz and current of 3 A) and without AMF exposure.

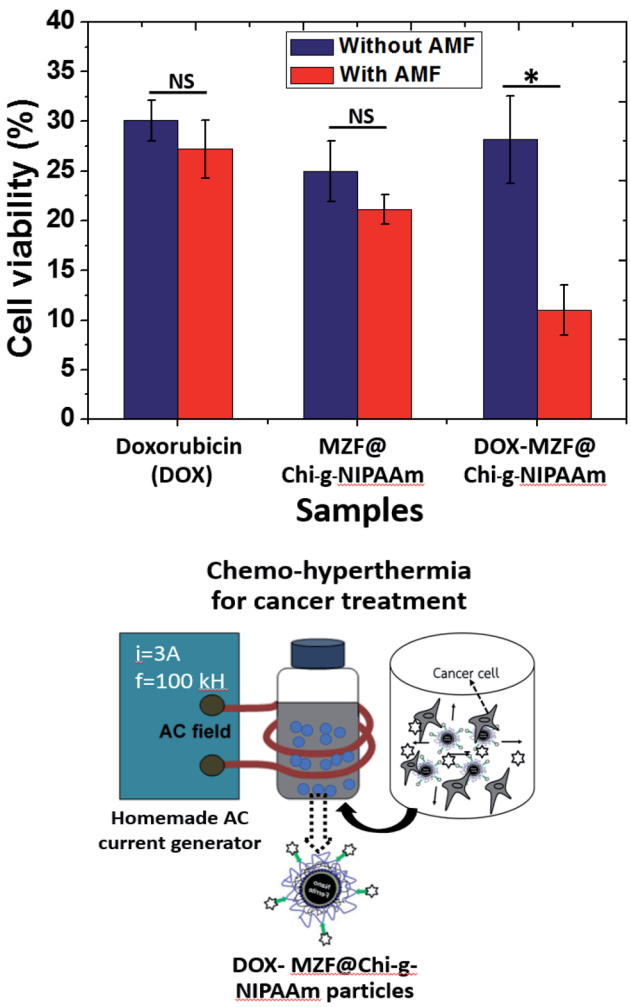

Fig. 6 Cell viability of HeLa cells of particles determined by MTT assay with and without exposure to an AMF ($f = 100$ kHz and current of 3 A). *$P < 0.05$, NS: no significance.

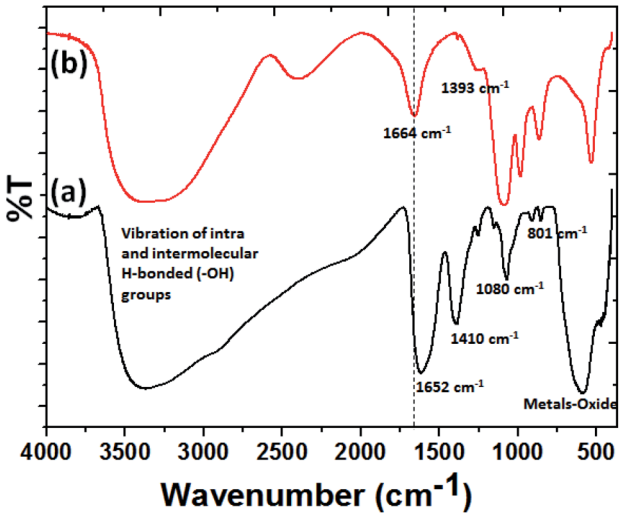

Fig. 7 FT-IR spectra of MZF@Chi-*g*-NIPAAm (a) and BMP-2-immobilized BSA loading MZF@Chi-*g*-NIPAAm particle (b).

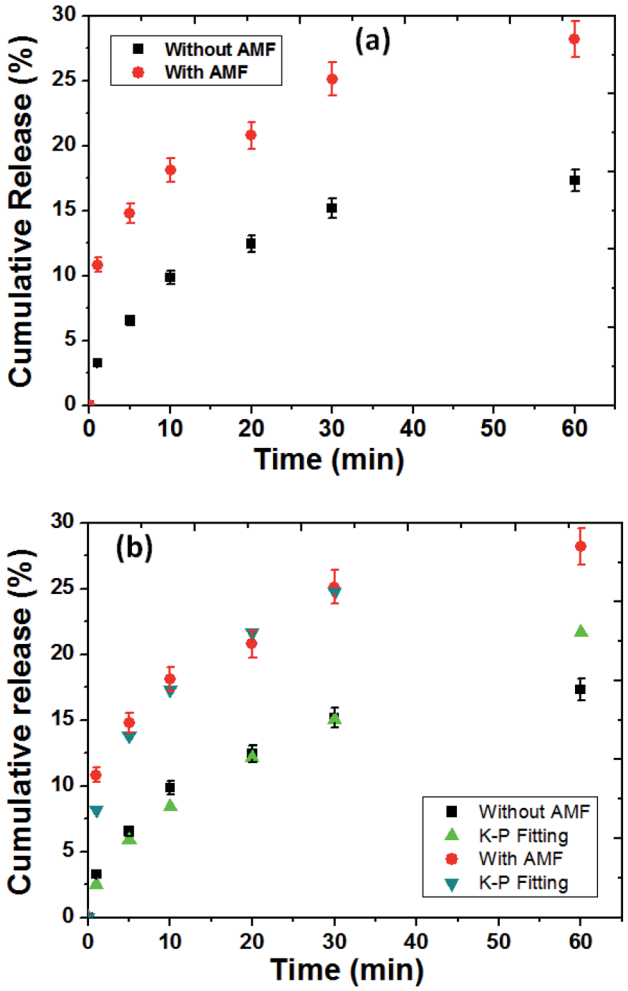

Fig. 8 The release profile of protein (BSA was used as protein model) from the P//MZF@Chi-*g*-NIPAAm particles were investigated in absence and presence of AMF stimulation (a). (b) Korsmeyer–Peppas kinetic models applied to the release of BSA from the P//MZF@Chi-*g*-NIPAAm particles.

NIPAAm particles were released for over the 1 h time period.-These results confirm the possibility of achieving the controlled magnetic release of drugs carried by MZF@Chi-*g*-NIPAAm particles. The significant enhanced protein release when applied by AMF compared with without magnetic field we assumed in this study that the alternating electromagnetic field influenced the ($(Mn,Zn)Fe_2O_4$) nanoparticles embedded in the Chi-*g*-NIPAAm polymer with superparamagnetism behavior. The oscillating magnetic field twisted the nanoparticles at a frequency corresponding to the frequency of the applied field causing this particle reorientation and simultaneously heat generation led to the disturbed structure of the polymer matrix as well as the surrounding BSA layer, which resulted in higher BSA release. Notably, the temperature from heat generation was about 36 °C and not changed during entire studied which is expected that protein was not denaturation (particularly protein denaturation occurred at around 60 °C). To describe the release behavior of BSA from P//MZF@Chi-*g*-NIPAAm particles, kinetics models of Korsmeyer–Peppas (K–P) has been chosen to examine the kinetics of release behavior of protein under with or without magnetic field exposure.

Fig. 8(b) shows the release data of BSA fitted with Korsmeyer–Peppas model,[41] according to the following equation $M_t/M_\alpha = Kt^n$, in which M_t and M_α are the cumulative amount of protein released at time t and the initial amount of protein present in the solution, respectively. K is release constant and n is the diffusional release exponent indicative of the release mechanism. When $n < 0.5$ then the drug release mechanism follows Fickian diffusion model.[42,43] and if $0.5 < n < 0.89$ then the release mechanism follows an anomalous diffusion model.[44] However, if $n = 0.5$ then the release mechanism follows Higuchi kinetic model.[42,43] It can be observed that the release profile of BSA up to 25.06% under AMF (for 30 min) and 15.16% without AMF has shown excellent fitting with K–P model with R^2 value of 0.990 and 0.977, respectively. The n values were found to be 0.32 and 0.53 for release of BSA for with and without AMF, respectively. The obtained n values for BSA release under AMF exposure was found to be lower than 0.5, suggesting the BSA release was followed by Fickian diffusion mechanism while without AMF, the values of n was in the range of $0.5 < n < 0.89$ indicating the release of BSA is governed by non Fickian diffusion (controlled by both swelling and Fickian diffusion process) process. The rate of release for BSA from P//MZF@Chi-*g*-NIPAAm particles under stimulated by AMF was higher than the absence AMF as indicated by the K values of 8.15 and 2.51 min^{-1}, respectively.

4. Conclusion

We synthesized and investigated MZF@Chi-*g*-NIPAAm particles as a drug and bioactive molecules delivery system and successfully DOX and BMP-2-immobilized BSA loading onto its surface. The MZF@Chi-*g*-NIPAAm particles provide the magnetic inductive heating ability that enable this system to treat cancer cells by hyperthermia and induce release of the

drug (around 58.9% within 20 min which is much higher compared without AMF exposure). The *in vitro* results reveal that DOX-MZF@Chi-*g*-NIPAAm particles exhibit high efficacy for cancer cells treatment in the presence of alternating magnetic field. This result suggests that 89.02% of cells were killed, as compared to 71.82% without AMF exposure. The results of the first stage (laboratory) testing suggest that DOX-loaded MZF@Chi-*g*-NIPAAm could be a potential drug delivery system and applicable for pH-stimuli responsive and magnetic hyperthermia in cancer treatment and therapy. In the vectoring delivery of protein, P//MZF@Chi-*g*-NIPAAm particle could be controlled by an AMF (magnetic actuation). Without magnetic field (physiological condition), BSA protein showed slowly release only 17.30% for over the 1 h time period and showed burst increase when applied with AMF. These results led to sustained release by with or without AMF exposure and have potential as vectoring delivery and controlled release of bioactive molecules for cancer treatment and cartilage or bone regenerative applications. Further *in vivo* (small animal) testing need to be done.

Conflicts of interest

There are no conflicts to declare.

Acknowledgements

The authors would like to acknowledge the financial support from Thailand Research Fund (TRF)-Office of the Higher Education Commission-Kasetsart University (RSA6080046, to W. P.), the Department of Physics, Faculty of Science, Kasetsart University (to W. M., W. P. and I. M. T.), and the National Nanotechnology Center, Thailand (to W. M.). I. M. T. would also like to acknowledge financial support provided by King Mongkut's University of Technology, Thonburi through the KMUTT 55th Anniversary Commemorative Fund.

References

1 T. Sun, Y. S. Zhang, B. Pang, D. C. Hyun, M. Yang and Y. Xia, Engineered nanoparticles for drug delivery in Cancer therapy, *Angew. Chem., Int. Ed.*, 2014, **53**, 12320–12364.

2 B. T. Mai, S. Fernandes, P. B. Balakrishnan and T. Pellegrino, Nanosystems Based on Magnetic Nanoparticles and Thermo- or pH Responsive Polymers: An Update and Future Perspectives, *Acc. Chem. Res.*, 2018, **51**, 999–1013.

3 J. Liao, Y. Jia, Y. Wu, K. Shi, D. Yang, P. Li and Z. Qian, Physical-, chemical-, and biological-responsive nanomedicine for cancer therapy, *WIREs Nanomed. Nanobiotechnol.*, 2019, e1581.

4 M. Sandhya, M. B. James, H. Alicia J El and T. Neil D, The potential of magnetic hyperthermia for triggering the differentiation of cancer cells, *Nanoscale*, 2018, **10**, 20519–20525.

5 W. Zhang, G. Yang, X. Wang, L. Jiang, F. Jiang, G. Li, Z. Zhang and X. Jiang, Magnetically Controlled Growth-Factor-Immobilized Multilayer Cell Sheets for Complex Tissue Regeneration, *Adv. Mater.*, 2017, **29**(43), 1703795.

6 G. Go, J. Han, J. Zhen, S. Zheng, A. Yoo, M. J. Jeon, J. O. Park and S. Park, A Magnetically Actuated Microscaffold Containing Mesenchymal Stem Cells for Articular Cartilage Repair, *Adv. Healthcare Mater.*, 2017, **6**(13), 1601378.

7 S. Z. M. Madani, A. Reisch, D. Roxbury and S. M. Kennedy, A Magnetically Responsive Hydrogel System for Controlling the Timing of Bone Progenitor Recruitment and Differentiation Factor Deliveries, *ACS Biomater. Sci. Eng.*, 2020, **6**, 1522–1534.

8 X. Liu, Y. Zhang, Y. Wang, W. Zhu, G. Li, X. Ma, Y. Zhang, S. Chen, S. Tiwari, K. Shi, S. Zhang, H. M. Fan, Y. X. Zhao and X. J. Liang, Comprehensive understanding of magnetic hyperthermia for improving antitumor therapeutic efficacy, *Theranostics*, 2020, **10**(8), 3793–3815.

9 S. Gao, G. Tang, D. Hua, R. Xiong, J. Han, S. Jiang, Q. Zhangd and C. Huang, Stimuli-responsive bio-based polymeric systems and their applications, *J. Mater. Chem. B*, 2019, **7**, 709–729.

10 S. Kaur, C. Prasad, B. Balakrishnan and R. Banerjee, Trigger responsive polymeric nanocarriers for cancer therapy, *Biomater. Sci.*, 2015, **3**, 955–987.

11 T. Kubo, K. Tachibana, T. Naito, S. Mukai, K. Akiyoshi, J. Balachandran and K. Otsuka, Magnetic Field Stimuli-Sensitive Drug Release Using a Magnetic Thermal Seed Coated with Thermal-Responsive Molecularly Imprinted Polymer, *ACS Biomater. Sci. Eng.*, 2019, **5**(2), 759–767.

12 X. Zhou, L. Wang, Y. Xu, W. Du, X. Cai, F. Wang, Y. Ling, H. Chen, Z. Wang, B. Hu and Y. Zheng, A pH and magnetic dual-response hydrogel for synergistic chemo-magnetic hyperthermia tumor therapy, *RSC Adv.*, 2018, **8**, 9812–9821.

13 E. C. Abenojar, S. Wickramasinghe, J. Bas-Concepcion and A. C. S. Sami, Structural effects on the magnetic hyperthermia properties of iron oxide nanoparticles, *Prog. Nat. Sci.: Mater. Int.*, 2016, **26**(5), 440–448.

14 N. D. Thorat, S. A. M. Tofail, B. von Rechenberg, H. Townley, G. Brennan, C. Sillien, H. M. Yadav, T. Seffen and J. Bauer, Physically stimulated nanotheranostics for next generation cancer therapy: Focus on magnetic and light stimulations, *Appl. Phys. Rev.*, 2019, **6**, 041306.

15 T. Kubo, K. Tachibana, T. Naito, S. Mukai, K. Akiyoshi, J. Balachandran and K. Otsuka, Magnetic Field Stimuli-Sensitive Drug Release Using a Magnetic Thermal Seed Coated with Thermal-Responsive Molecularly Imprinted Polymer, *ACS Biomater. Sci. Eng.*, 2019, **5**(2), 759–767.

16 X. Zhou, L. Wang, Y. Xu, W. Du, X. Cai, F. Wang, Y. Ling, H. Chen, Z. Wang, B. Hu and Y. Zheng, A pH and magnetic dual-response hydrogel for synergistic chemo-magnetic hyperthermia tumor therapy, *RSC Adv.*, 2018, **8**, 9812–9821.

17 M. Sandhya, M. B. James, H. Alicia J. El and T. Neil D, The potential of magnetic hyperthermia for triggering the differentiation of cancer cells, *Nanoscale*, 2018, **10**, 20519–20525.

18 M. Walker, I. Will, A. Pratt, V. Chechik, P. Genever and D. Ungar, Magnetically Triggered Release of Entrapped Bioactive Proteins from Thermally Responsive Polymer-Coated Iron Oxide Nanoparticles for Stem-Cell Proliferation, *ACS Appl. Nano Mater.*, 2020, **3**, 5008–5013.

19 M. Fan, J. Yan, H. Tan, Y. Miao and X. Hu, Magnetic biopolymer nanogels via biological assembly for vectoring delivery of biopharmaceuticals, *J. Mater. Chem. B*, 2014, **2**, 8399–8405.

20 J. R. Henstock, M. Rotherham, H. Rashidi, K. M. Shakesheff and A. J. El Haj, Remotely Activated Mechanotransduction via Magnetic Nanoparticles Promotes Mineralization Synergistically With Bone Morphogenetic Protein 2: Applications for Injectable Cell Therapy, *Stem Cells Transl. Med.*, 2014, **3**, 1363–1374.

21 D. Honarmand, S. M. Ghoreishi, N. Habibi and E. T. Nicknejad, Controlled release of protein from magnetite–chitosan nanoparticles exposed to an alternating magnetic field, *J. Appl. Polym. Sci.*, 2016, **133**, 43335.

22 B. Sung, S. Shaffer, M. Sittek, T. Alboslemy, C. Kim and K. Min-Ho, Alternating Magnetic Field-Responsive Hybrid Gelatin Microgels for Controlled Drug Release, *J. Visualized Exp.*, 2016, **108**, e53680.

23 Q. Yang, L. Jianbo, R. Jie, L. Junzhao, L. Chao and S. Donglu, Enhanced Magnetic Fluid Hyperthermia by Micellar Magnetic Nanoclusters Composed of $Mn_xZn_{1-x}Fe_2O_4$ Nanoparticles for Induced Tumor Cell Apoptosis, *ACS Appl. Mater. Interfaces*, 2014, **6**(19), 16867–16879.

24 J. Xie, Y. Zhang, C. Yan, L. Song, S. Wen, F. Zang, G. Chen, Q. Ding, C. Yan and N. Gu, High-performance PEGylated Mn-Zn ferrite nanocrystals as a passive-targeted agent for magnetically induced cancer theranostics, *Biomaterials*, 2014, **35**(33), 9126–9136.

25 J. Xie, C. Yan, Yu Yan, L. Chen, L. Song, F. Zang, Y. An, G. Teng, N. Gu and Y. Zhang, Multi-modal Mn-Zn ferrite nanocrystals for magnetically-induced cancer targeted hyperthermia: a comparison of passive and active targeting effects, *Nanoscale*, 2016, **8**, 16902–16915.

26 N. Jović Orsini, M. M. Milić and T. E. Torres, Zn- and (Mn, Zn)-substituted *versus* unsubstituted magnetite nanoparticles: Structural, magnetic and hyperthermic properties, *Nanotechnology*, 2020, **31**(22), 225707.

27 Y. Sun, C. Yan, J. Xie, D. Yan, K. Hu, S. Huang, J. Liu, Y. Zhang, N. Gu and F. Xiong, High-Performance Worm-like Mn-Zn Ferrite Theranostic Nanoagents and the Application on Tumor Theranostics, *ACS Appl. Mater. Interfaces*, 2019, **11**, 29536–29548.

28 C. Alvarez-Lorenzo, A. Concheiro, A. S. Dubovik, N. V. Grinberg, T. V. Burova and V. Y. Grinberg, Temperature-sensitive chitosan-poly(N-isopropylacrylamide) interpenetrated networks with enhanced loading capacity and controlled release properties, *J. Controlled Release*, 2005, **102**, 629–641.

29 C. Echeverria, P. Soares, A. Robalo, L. Pereira, C. M. M. Novo, I. Ferreira and J. P. Borges, One-pot synthesis of dual-stimuli responsive hybrid PNIPAAm-chitosan microgels, *Mater. Des.*, 2015, **86**, 745–751.

30 M. K. Jaiswal, R. Banerjee, P. Pradhan and D. Bahadur, Thermal behavior of magnetically modalized poly(N-isopropylacrylamide)-chitosan based nanohydrogel, *Colloids Surf., B*, 2010, **81**, 185–194.

31 W. J. King and P. H. Krebsbach, Growth factor delivery: How surface interactions modulate release in vitro and in vivo, *Adv. Drug Delivery Rev.*, 2012, **64**, 1239–1256.

32 Z. Wang, Z. Wang, W. W. Lu, W. Zhen, D. Yang and S. Peng, Novel biomaterial strategies for controlled growth factor delivery for biomedical applications, *NPG Asia Mater.*, 2017, **9**, e435.

33 F. M. Chen, M. Zhang and Z. F. Wu, Toward delivery of multiple growth factors in tissue engineering, *Biomaterials*, 2010, **31**, 6279–6308.

34 W. Montha, W. Maneeprakorn, N. Buatong, I. M. Tang and W. Pon-On, Synthesis of doxorubicin-PLGA loaded chitosan stabilized (Mn, Zn)Fe_2O_4 nanoparticles: Biological activity and pH-responsive drug release, *Mater. Sci. Eng., C*, 2016, **59**, 235–240.

35 M. Angelakeris, Magnetic nanoparticles: a multifunctional vehicle for modern theranostics, *Biochim. Biophys. Acta*, 2017, **1861**, 1642–1651.

36 E. C. Abenojar, S. Wickramasinghe, J. Bas-Concepcion and A. C. S. Sami, Structural effects on the magnetic hyperthermia properties of iron oxide nanoparticles, *Prog. Nat. Sci.: Mater. Int.*, 2016, **26**(5), 440–448.

37 J. Mohapatra, M. Xing and J. P. Liu, Inductive Thermal Effect of Ferrite Magnetic Nanoparticles, *Materials*, 2019, **12**, 3208.

38 J. Kong and S. Yu, Fourier Transform Infrared Spectroscopic Analysis of Protein Secondary Structures, *Acta Biochim. Biophys. Sin.*, 2007, **39**, 549–559.

39 S. Sahoo, C. Chakraborti, P. Behera and S. Mishra, FTIR and Raman Spectroscopic Investigations of a Norfloxacin/Carbopol934 Polymeric Suspension, *J. Young Pharm.*, 2012, **4**, 138–145.

40 E. J. Milner-White, The Partial Charge of the Nitrogen Atom in Peptide Bonds, *Protein Sci.*, 1997, **6**, 2477–2482.

41 N. A. Peppas, Analysis of Fickian and non-Fickian drug release from polymers, *Pharm. Acta Helv.*, 1985, **60**(4), 110–111.

42 D. Y. Arifin, L. Y. Lee and C. H. Wang, Mathematical modeling and simulation of drug release from microspheres: implications to drug delivery systems, *Adv. Drug Delivery Rev.*, 2006, **58**, 1274–1325.

43 J. Siepmann and F. Siepmann, Mathematical modeling of drug delivery, *Int. J. Pharm.*, 2008, **364**, 328–343.

44 P. Costa and J. M. S. Lobo, Modeling and comparison of dissolution profiles, *Eur. J. Pharm. Sci.*, 2001, **13**, 123–133.

